Celestial Mechanics and Dynamical Astronomy (2005) 92:243–255
DOI 10.1007/s10569-004-3834-6

LOCAL AND GLOBAL DIFFUSION ALONG RESONANT LINES IN DISCRETE QUASI-INTEGRABLE DYNAMICAL SYSTEMS

CLAUDE FROESCHLÉ[1], MASSIMILIANO GUZZO[2] and ELENA LEGA[1]
[1]*Observatoire de Nice, Bv. de l'Observatoire, B.P. 4229, 06304 Nice cedex 4, France, e-mail: elena@obs-nice.fr*
[2]*Dipartimento di Matematica Pura ed Applicata, Università degli Studi di Padova, via Belzoni 7, 35131 Padova, Italy.*

(Received: 5 July 2004; revised: 20 September 2004; accepted: 23 September 2004)

Abstract. We detect and measure diffusion along resonances in a quasi-integrable symplectic map for different values of the perturbation parameter. As in a previously studied Hamiltonian case (Lega et al., 2003) results agree with the prediction of the Nekhoroshev theorem. Moreover, for values of the perturbation parameter slightly below the critical value of the transition between Nekhoroshev and Chirikov regime we have also found a diffusion of some orbits along macroscopic portions of the phase space. Such a diffusion follows in a spectacular way the peculiar structure of resonant lines.

Key words: Global diffusion, Quasi-integrable Dynamical Systems

1. Introduction

In order to highlight the possibility of a drift of the actions along a resonance in an Hamiltonian quasi-integrable system. Arnold (1964) built an ad hoc model showing the existence of a very slow diffusion. This kind of diffusion is very difficult to detect numerically.

Within the framework of Nekhoroshev's (1977) theorem, one expects an exponentially slow drift of the actions along resonant lines. Moreover, the speed of the diffusion decreases as the order of the resonance increases (Morbidelli and Giorgilli, 1995; Giorgilli and Morbidelli, 1997).

In a previous work (Lega et al., 2003), using a time dependent Hamiltonian system with two degrees of freedom, we have provided numerical evidence for the existence of diffusive orbits along resonances as well as numerical estimate of the diffusion coefficient as a function of the perturbing parameter. The decreasing of the diffusion coefficient with the perturbing parameter is stronger than a power law, typical of Chirikov (1979) diffusion, and is compatible with an exponential law as expected in the Nekhoroshev regime.

In this paper, we perform the same kind of numerical experiments on a quasi-integrable symplectic mapping T of dimension four with a non integrable part analogous to that of the Hamiltonian used in Lega et al. (2003). Initial conditions were taken in the chaotic zone of a selected resonance. Such

orbits were chosen using the fast Lyapunov indicator (FLI, Froeschlé and Lega, 2000), which allows to have a detailed knowledge of the topology of the resonances.

The use of the FLI allows to determine (Guzzo et al., 2002) both for slightly perturbed Hamiltonian systems and for weakly coupled symplectic mappings, the critical value of the perturbing parameter that corresponds to the transition from a Chirikov regime to the Nekhoroshev one. Therefore, chaotic initial conditions were taken for values of the coupling parameter still in the Nekhoroshev regime but relatively close to such a critical value.

The same procedure is applied in the present paper to the detection of the diffusion in the mapping T. The results obtained for the mapping are both qualitatively and quantitatively similar to those obtained for the Hamiltonian system in agreement with recent proofs of the Nekhoroshev theorem for nearly integrable symplectic maps (Kuksin and Pöschel, 1994; Guzzo, 2004). Moreover, thanks to the rapid computation of the mapping, which allows to explore much longer integration times with respect to the Hamiltonian system we have observed that Arnold's diffusion is relevant for global diffusion (Guzzo et al., 2005). More precisely, for a suitable choice of the perturbation parameter we show that a global diffusion occurs along the peculiar set of resonances forming the Arnold's web.

The paper is organized as follows. We recall in Section 2 the definition of the FLI and we give an application to the symplectic 4 dimensional map. We provide in Section 3 the evidence of the diffusion along resonant lines. The numerical estimate of the diffusion coefficient will be given in Section 4. Section 5 is devoted to the phenomenon of global Arnold's diffusion. Conclusions are provided in Section 6.

2. The FLI Revisited

When computing the Lyapunov characteristics indicators (LCI), the attention is focused on the length of time necessary to get a reliable value of their limit, but very little importance is given to the first part of the computation. In fact, this part is considered as a kind of transitory regime depending, among other factors, on the choice of an initial vector of the tangent manifold.

Already Froeschlé et al. (1997) have remarked that the intermediate value of the LCI (which was called FLI), taken at equal times for chaotic (even slow chaotic) and ordered motion, allows to distinguish between them. It turns out that the FLI allows also to distinguish among ordered motions of different origins, like resonant and non-resonant motions (Guzzo et al., 2002), despite the fact that in both cases the largest LCI tends to zero when time goes to infinity.

2.1. DEFINITION OF THE FLI

Given a mapping M from $\mathbb{R}^n$ to $\mathbb{R}^n$ an initial condition $\vec{x}(0) \in \mathbb{R}^n$, and an initial vector $\vec{v}(0) \in \mathbb{R}^n$ of norm 1 (we remark that in this particular case the manifold and the tangent manifold are both $\mathbb{R}^n$), let us define the FLI function $F(\vec{x}(0), \vec{v}(0), \tau), \tau$ belonging to $\mathbb{Z}^+$, as:

$$F(\vec{x}(0), \vec{v}(0), \tau) = \sup_{0<t\leqslant\tau} \log \|\vec{v}(t)\| \tag{1}$$

where $v(t)$ is given by the system:

$$\begin{cases} \vec{x}(t+1) = M\vec{x}(t) \\ \vec{v}(t+1) = \frac{\partial M}{\partial \vec{x}}(\vec{x}(t))\vec{v}(t) \end{cases} \tag{2}$$

Let us remark that this definition has replaced, since Froeschlé et al.(2000), the first one given in Froeschlé et al. (1997). With the actual definition we could get rid of unnecessary complications and the introduction of the supremum of the norm has the same advantage of an averaging procedure easier to handle. Moreover the present definition is especially suited to the analysis of the neighborhood of a periodic orbit (Froeschlé and Lega, 2005).

2.2. A FOUR DIMENSIONAL MAP AS A MODEL PROBLEM

In previous papers (Froeschlé et al., 2000; Guzzo et al., 2002; Lega et al., 2003) we used the FLI to describe the geometry of the resonances of the Hamiltonian system:

$$H = \frac{I_1^2}{2} + \frac{I_2^2}{2} + I_3 + \epsilon \frac{1}{\cos(\phi_1) + \cos(\phi_2) + \cos(\phi_3) + 4} \tag{3}$$

where $I_1, I_2, I_3 \in \mathbb{R}$ and $\phi_1, \phi_2, \phi_3 \in \mathbb{T}$ are canonically conjugate and ϵ is a small parameter.

In this paper we use the FLI for the same kind of studies, for a symplectic mapping obtained through the leap-frog discretization (which ensures the symplecticity of the mapping) of the equations of motion of Equation (3):

$$T = \begin{cases} x_{j+1} = & x_j - \epsilon \frac{\sin(x_j+y_j)}{(\cos(x_j+y_j)+\cos(z_j+t_j)+4)^2} & \\ y_{j+1} = & y_j + x_j & (\mathrm{mod} 2\pi) \\ z_{j+1} = & z_j - \epsilon \frac{\sin(z_j+t_j)}{(\cos(x_j+y_j)+\cos(z_j+t_j)+4)^2} & \\ t_{j+1} = & z_j + t_j & (\mathrm{mod} 2\pi) \end{cases} \tag{4}$$

We still have a quasi-integrable system with the usual advantage of mappings: we can integrate for times longer than in the continuous case and this fact is crucial when dealing with the diffusion for small values of ϵ.

Figure 1 shows the variation of the FLI with time for three different kinds of orbits of T (indicated by arrows in Figure 2) with $\epsilon = 0.6$. The upper curve, with initial conditions in a chaotic zone in Figure 2: $(x = 2.07, y = 0, z = 2.1, t = 0)$ shows an exponential increase of the FLI with time. The intermediate curve corresponds to a regular invariant torus of initial conditions $(x = 1.8, y = 0, z = 1.2, t = 0)$ and the lowest one corresponds to a regular resonant curve of initial conditions $(x = 1.67, y = 0, z = 0.91, t = 0)$. Although the largest Lyapunov exponent of the two regular curves above is zero, the FLI, as shown in Figure l, distinguishes between resonant and non resonant regular motions. More precisely, although the two curves exhibit essentially the same behavior they are parallel but distinct. At the origin of the different values of the FLI for regular non resonant and resonant motion there is the differential rotation which is not the same for the two dynamics. The FLI behavior has been extensively studied both numerically and analytically in (Guzzo et al., 2002).

Figure 2 shows, at $\tau = 1000$, the FLI for a grid of 500×500 initial conditions regularly spaced on x, z. The other initial conditions are $y = 0, t = 0$, and the initial vector is $\vec{v}(0) = (0.5(\sqrt{3} - 1), 1, 1, 1)$. The FLI is reported with a grey scale: the dark strips correspond to regular resonant

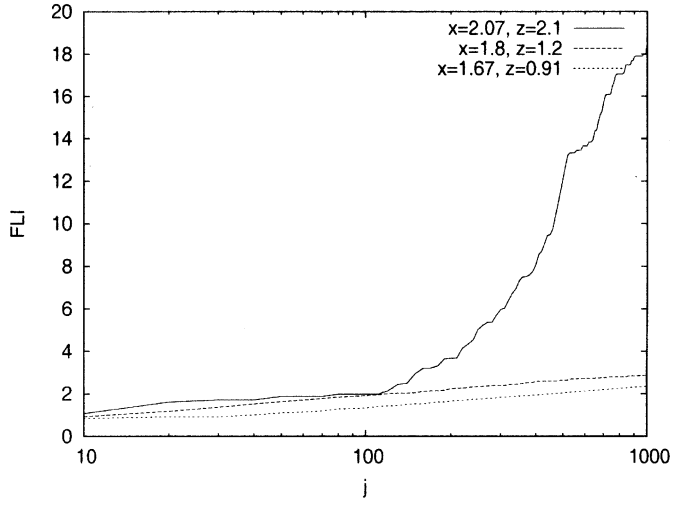

Figure 1. Variation of the FLI as a function of time for three orbits of the standard map T with $\epsilon = 0.6$. The upper curve is for a chaotic orbit with initial conditions ($x = 2.07$, $y = 0$, $z = 2.1$, $t = 0$) the middle one is for a regular non resonant orbit with ($x = 1.8$, $y = 0$, $z = 1.2$, $t = 0$) and the lowest one is for a regular resonant orbit with ($x = 1.67$, $y = 0$, $z = 0.91$, $t = 0$).

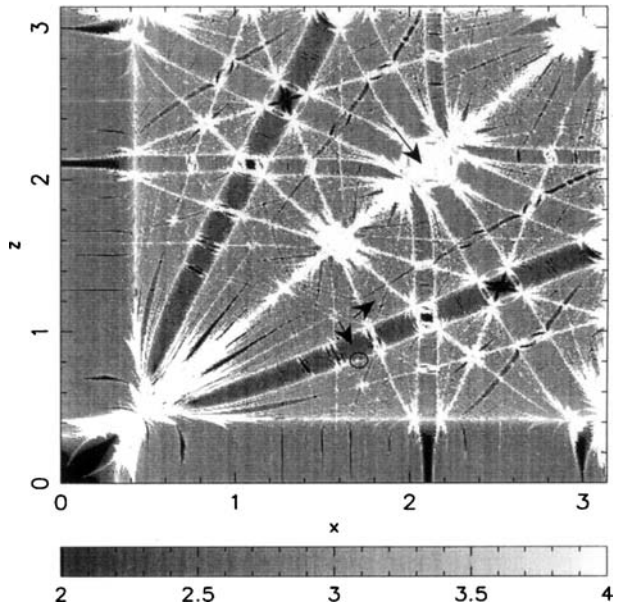

Figure 2. Geography of resonances in the plane $x - z$ for the mapping T with $\epsilon = 0.6$. The computation has been done for a set of 500×500 initial conditions regularly spaced on x, z. The other initial conditions are $y = 0, t = 0$, and the initial vector is $\vec{v} = (0.5(\sqrt{3} - 1), 1, 1, 1,)$. The grey scale ranges from black ($FLI \leqslant 2$) to white ($FLI \geqslant 4$).

motions while the white lines represent both chaotic resonant motions or the vicinity of a separatrix. The orbits having an FLI value of about $\log(\tau)$ constitute the background of KAM tori. Let us remark that for the Hamiltonian of Equation (3), when $\epsilon = 0$ the frequencies are strictly equal to the actions, therefore the FLI charts are nothing but frequencies charts, which display a very well detailed Arnold's web.

As far as the mapping is concerned, the same occurs when considering the variables $x(j)$ and $z(j)$ which are the frequencies of the unperturbed mapping $T(\epsilon = 0)$. Again, the FLI chart in the plane r–z (Figure 2) shows very clearly the Arnold's web.

3. Diffusion Along Resonances: Qualitative Aspects

For the four dimensional symplectic mapping T we have computed the FLI charts for different values of the perturbing parameter and we have selected a low order resonance. In order to compare the results obtained in the case of the Hamiltonian system of Equation 3 we have considered the same unperturbed resonance $x = 2z$.

Using the method of the FLI charts described in Froeschlé et al. (2000) and in Guzzo et al. (2002) we found that the critical perturbation parameter for the transition between the Nekhoroshev and the Chirikov regime is in the interval $0.8 < \epsilon < 1$.

Starting from an upper bound of $\epsilon = 0.7$, we have looked for diffusive orbits in the Nekhoroshev regime.

Figure 3 shows the FLI charts of the actions space for successive zoom around $x = 1.7$, $z = 0.8$ for different values of ϵ. In these pictures the region between the two white lines is the resonant strip approximated by $x - 2z < \sqrt{\epsilon}$, and the two white lines correspond to its hyperbolic border where diffusion is confined. These charts provide us the possibility of choosing initial conditions in the hyperbolic border. Then, we can also follow the evolution of the corresponding orbits on the FLI charts by plotting the points which intersect the double section $\sigma = |y| + |t| \leqslant 0.005$. Let us remark, that in such a way we minimize all projection effects and fast quasi-periodic movements. What remains is a very slow drift along the border of the resonance.

We have taken a set of 100 initial conditions corresponding to orbits of the FLI charts having FLI values larger than $1.5 \log(\tau)$, i.e., to chaotic orbits at the border of the resonance, far from the more stable crossing with other resonances. We have plotted on the FLI charts all the points in the double section described above. We remark that such points will appear on both side of the resonance (in fact the two white lines are connected by an hyperbolic region in the 4 dimensional phase space).

We show for $\epsilon = 0.6$, the evolution of the 100 orbits up to $j = 6 \times 10^6$ Figure 3 (top, left) and up to $j = 3 \times 10^8$ Figure 3(top, right). The diffusion along the resonance appears clearly, although the higher order resonances intersecting the main one become evident, and consequently the region of diffusion extends a little also on the direction transversal to the resonance.

When decreasing the perturbation, $\epsilon = 0.2$, the diffusion along the resonant line is more clear. In Figure 3 (middle) we have plotted again the intersections of the 100 orbits with the double section σ on the FLI chart after respectively $j = 3 \times 10^8$ (middle. left) and $j = 2 \times 10^{10}$ (middle, right). The phenomenon still appears very clearly even for $\epsilon = 0.07$, Figure 3 (bottom). i.e., an order of magnitude lower than the threshold of transition between the two regimes. We have observed the phenomenon down to $\epsilon = 0.03$.

4. Diffusion Along Resonances: Quantitative Aspects

In order to measure the diffusion coefficient we have considered the phenomenon as if it was a Brownian motion, since we do not have yet an analytic

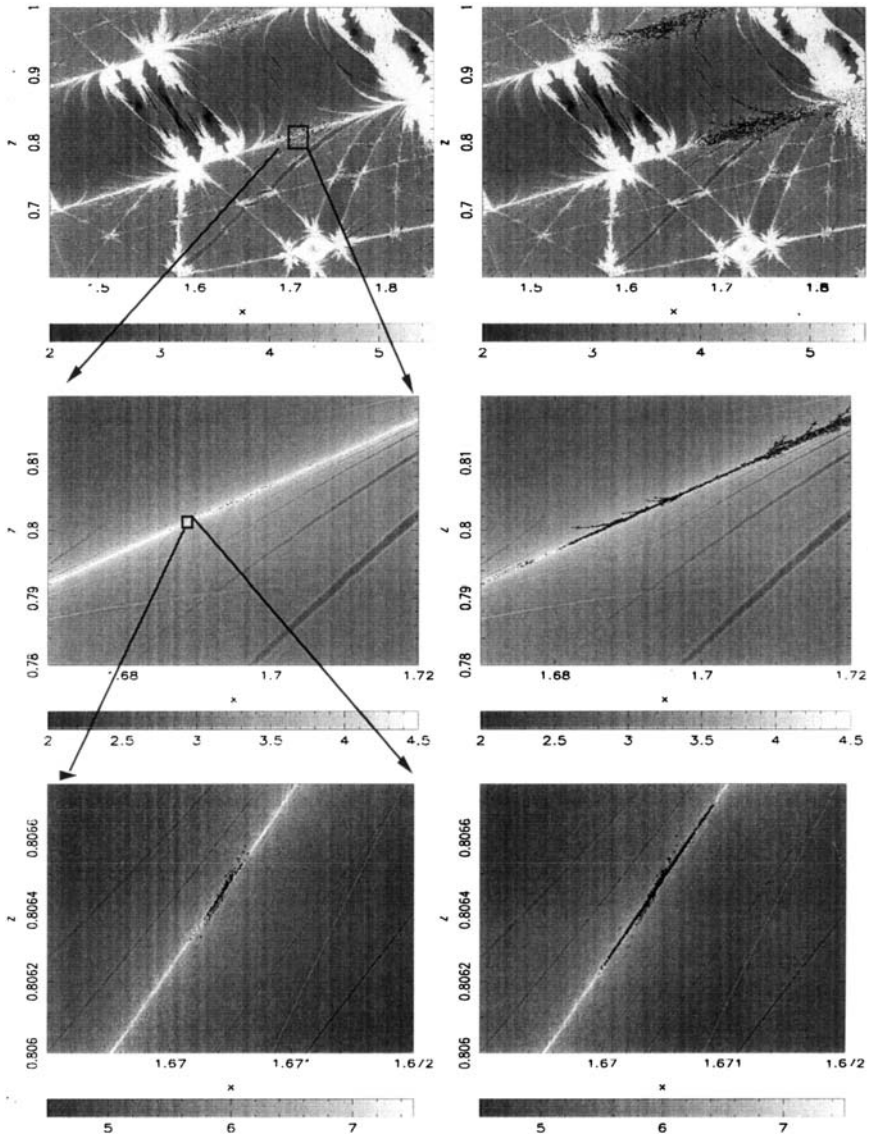

Figure 3. Diffusion along the resonant line $x = 2z$ of the mapping T for $\epsilon = 0.6$ (top), $\epsilon = 0.2$ (middle), $\epsilon = 0.07$ (bottom) for a set of 100 initial conditions taken in the chaotic border of the resonance. The figure in the middle and in the bottom correspond to the zone of the phase space contained in the square plotted respectively in the figure at top, left and in the figure at middle, left. The black points are the intersections of the orbits with the double section $|y| + |t| \leqslant 0.005$. The number of iterations on the set of orbits are respectively: $j = 6 \times 10^6$(top, left). $j = 3 \times 10^8$ (top, right). 3×10^8 (middle, left). 2×10^{10} (middle, right). 2×10^9 (bottom, left). 2.5×10^{10} (bottom, right). The grey scale ranges from black to white.

model for a diffusion like the one we observed. We look therefore for a linear increase with time of the mean square distance from the initial conditions. We are aware that this is a very crude assumption and that for systems like the standard map diffusion can be anomalous for very high values of the perturbation parameter Zaslavski and Edelman (2000), where no invariant curves remain. Instead, our computations concern quasi-integrable cases. This is a very interesting problem which goes behind the purpose of the present paper, mostly because we are submitted to computational limitations: we can't take a very large number of initial conditions which would require very long CPU times.

Notwithstanding these difficulties, we observed indeed an averaged linear increase with time of the mean squared distance from the initial conditions. Moreover, in order to reduce the contributions due to fast motion, we have only taken into account the points on the double section. More precisely, denoting with $x_i(0)$ and $z_i(0), i = 1, \ldots, N$ the initial conditions of a set of N orbits, with $x_i(j)$ and $z_i(j)$ the corresponding values at time j, and choosing a fraction t^* of the total integration time, we considered the quantity:

$$S(nt^*) = \frac{1}{M_n} \sum_{i:(|y_i(j)|+|t_i(j)|)<0.005} [(z_i(j) - 2x_i(j)) - (z_i(0) - 2x_i(0))]^2 \qquad (5)$$

where M_n is the number of points on the double section for j in the interval $(n-1)t^* \leqslant j \leqslant nt^*$. We observe (Figure 4) a linear increase with time of S and we estimate the diffusion coefficient D as the slope of the regression line.

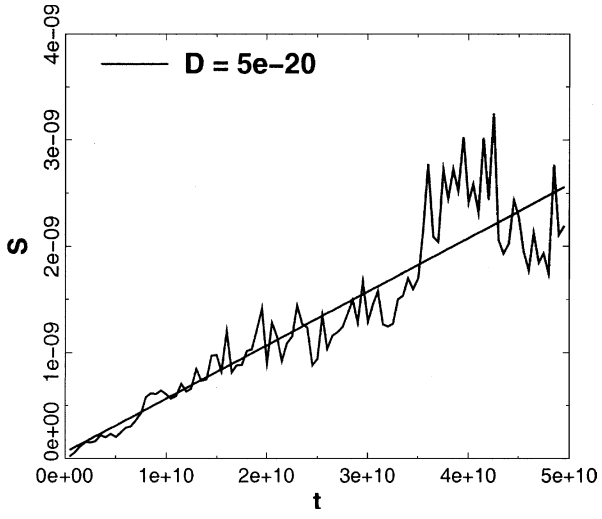

Figure 4. Evolution of the quantity $\bar{S}(nt^*)$ (see text) with $t^* = 5 \times 10^8$, for 100 orbits of the mapping T with $\epsilon = 0.05$. The slope of the regression line gives the diffusion coefficient $D = 5 \times 10^{-20}$.

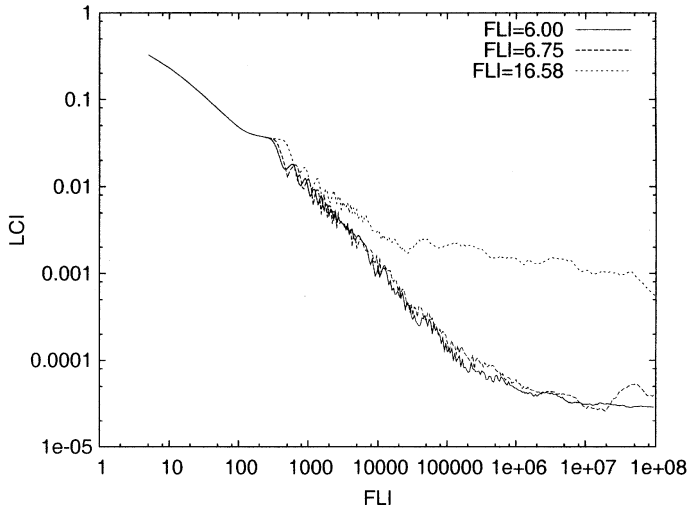

Figure 5. Evolution of the largest Lyapunov indicator with time for three orbits of the standard map T with $\epsilon = 0.05$. The initial conditions are $x = 1.67209489949749$ $y = 0.$ $z = 0.809297781072027$ $t = 0 (FLI = 6.0)$, $x = 1.67192854271357$ $y = 0.$ $z = 0.809236608877722$ $t = 0. (FLI = 6.75), x = 1.67203944723618$ $y = 0.$ $z = 0.809286279229481$ $t = 0. (FLI = 16.58)$.

Following Zaslavski and Edelman (2001), we could have diffusion, more precisely anomalous diffusion, driven by orbits with zero Lyapunov exponent. Moreover, since the initial conditions were chosen using the FLI computed on a relatively short time we have checked the chaotic character of some of the selected orbits by computing the largest Lyapunov exponent. More precisely, we computed the Lyapunov indicators. i.e. the truncated values of the Lyapunov exponents which are defined by a limit for time going to infinity.

Figure 5 shows the evolution with time of the largest Lyapunov indicator of three orbits for $\epsilon = 0.05$. The orbits have been chosen considering the FLI distribution of the 100 initial conditions: the first one has the lowest FLI (6.00), the second has an FLI in the middle of the distribution (6.75) while the third has the largest FLI value (16.58). We recall that the FLI chart for $\epsilon = 0.05$ was computed on $\tau = 10^4$ iterations and that the orbits are considered chaotic when they have $FLI \geqslant 1.5 \log \tau$, i.e., $FLI \geqslant 6$ in the considered case. For the three-test orbits the largest Lyapunov indicator is small but positive (Figure 5) ensuring that we are following very weak chaotic motions. This kind of test comforts our confidence in using FLI method for distinguishing the dynamical character of the orbits on times which may be even some order of magnitude shorter than the time needed for the Lyapunov indicators to stop to decrease and to stabilize at a positive value.

The estimates of $ln(D)$ versus $ln(1/\epsilon)$ are reported in Figure 6. We have defined three sets of data, performing a local regression for each of them of the form $ln(D) = a + m\ln(1/\epsilon)$, and found three different slopes. The first set contains the values of D for $\ln(1/\epsilon) \leqslant 0.92$, the second for $1.17 \leqslant \ln(1/\epsilon) \leqslant 2.28$ and the third for $\ln(1/\epsilon) \geqslant 2.43$, and the corresponding slopes are respectively $m_1 = -4.2$, $m_2 = -8.5$ and $m_3 = -13.3$. Such changes of slope comfort the expected exponential decrease of D, as for the Hamiltonian case reported in (Lega et al., 2003).

It would be natural at this point to check if the exponential upper bound $D < \exp -(1/\epsilon)^b$ expected from Nekhoroshev theorem can be seen from our data, and in particular if one can obtain a numerical estimation of b. Indeed, an exponential fit of our data would give the value $b = 0.28$ (Figure 6) with apparently very good correlation coefficient of about 0.99. However, how much this computation is meaningful is a delicate matter: the apparently good correlation coefficient is due mainly to the small interval in ϵ used for the exponential fit (Figure 6): there are not theoretical predictions to compare to the detected value: numerical studies (Benettin and Fassó, 1999) have shown that the exponential upper bounds found by perturbation theories are indeed only upper bounds, while the true exchange of energy among the different degrees of freedom with respect to a perturbing parameter typically follows more complicated functional laws. For these reasons, we think it is necessary in the future to perform more numerical studies of the problem.

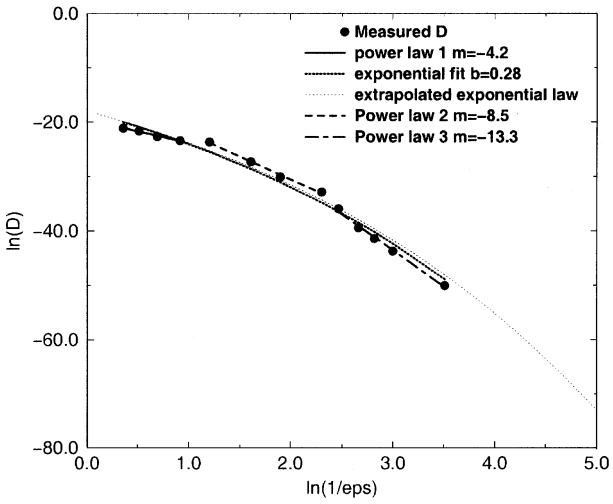

Figure 6. The logarithm of diffusion coefficient is plotted as a function of $\ln(1/\epsilon)$. The change of slope of the three power law fits is in agreement with the expected exponential decrease of D.

5. Global Diffusion

In the previous sections we have clearly showed the phenomenon of Arnold's diffusion occurring along a resonant line. It is clearly a phenomenon of local diffusion. When dealing with global diffusion we immediately think to the well known Chirikov's diffusion, due to the overlapping of resonances. Is it the only mechanism for global diffusion? At this purpose we have repeated the previous experiments for a given value of the perturbation parameter, close to the transition to the Chirikov regime, on a very long interval of time. We have considered twenty initial conditions in the vicinity of the point $(x, z) = (1.71,\ 0.81)$ for the symplectic map. Then, we computed numerically the map up to 10^{11} iterations.

The results are reported in Figure 7. Figure 7a shows only the location of initial conditions (inside the circles), on the FLI map of the action plane $(x,\ z)$, Figure 7a shows that we are in the Nekhoroshev regime since the resonances do not overlap and the majority of the orbits, i.e. dark grey and black zones in the FLI-chart, are regular. In Figure 7b we plotted as black dots all points of the orbits which have returned after some time on the section $|y| + |t| \leqslant 0.005$. We observe that the orbits filled a macroscopic region of the action plane whose structure is clearly that of the Arnold web (Guzzo et al., 2005). The orbits have moved along the single resonances, and avoided the center of the main resonance crossings, in agreement with the theoretical results which predict longer stability times for motions in these regions. The larger resonances (which correspond to the smaller orders) are practically all visited, while this is not the case for the thiner ones (which correspond to the higher orders). This is in agreement with the theoretical results of (Morbidelli and Giorgilli, 1995; Giorgilli and Morbidelli, 1997), which predict that the speed of diffusion on each resonance becomes smaller for resonances of high order. Therefore, the possibility of visiting all possible resonances is necessarily limited by finite computational time.

The described diffusion phenomenon is very different from Chirikov diffusion which is illustrated in Figure 7c, where the overlapping of resonances appears clearly since, except for the large strip of regular resonant zones corresponding to $x = 0$ and to $z = 0$, almost all regular orbits have disappeared. In the FLI-chart we observe a large white sea with small dark grey or black islands. In this case the diffusion for 20 initial conditions located in the circle of Figure 7c occurs in the same macroscopic region of Figure 7b of the phase space in a much shorter time scales (only $2{\times}10^7$ iterations) and without apparent peculiar topological properties of the stochastic region, i.e. the whole chaotic sea is densely visited.

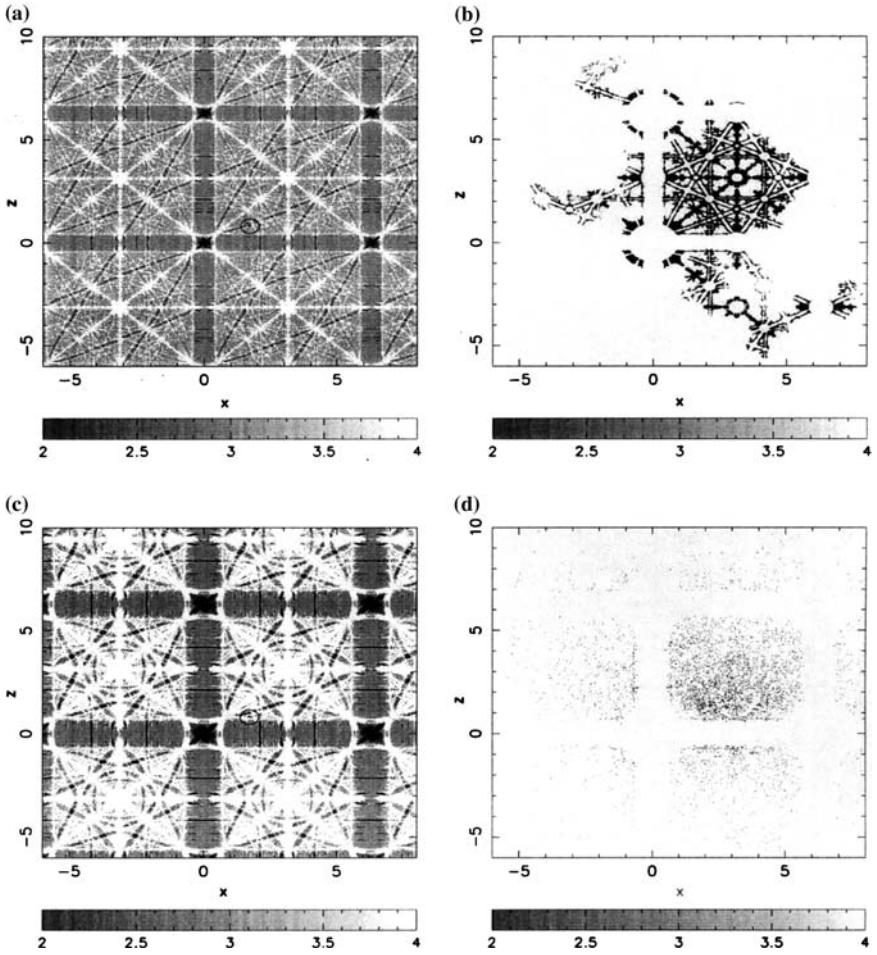

Figure 7. Panels (a) and (c) correspond to the FLI map of the action plane (x, z) for the map T for $\epsilon = 0.6$(a) and $\epsilon = 1.7$. The white region correspond to the chaotic part of the Arnold web. We marked with a circle the location of the twenty initial conditions chosen in the vicinity of the point $(x, z) = (1.71, 0.81)$. In panels (b) and (d) we marked with a black dot all points of the twenty orbits which have returned after some time on the section $|y| + |t| < 0.005$. We consider 10^{11} iterations for panel (b) and 2×10^7 iterations for panel (d).

6. Conclusion

By using a sensitive tool, the FLI, to detect the geography of resonances, we have been able to choose and follow orbits which exhibit diffusive behavior along resonant lines on a 4 dimensional symplectic map. We do not have an analytic model for such a diffusion, thus we make the hypothesis that it behaves as a Brownian motion. Under this hypothesis we measured a

diffusion coefficient and showed that the dependence of the diffusion coefficient on the perturbing parameter does not follow a power law, and in the explored range is in agreement with the exponential decay predicted by Nekhoroshev theory. Results agree with those previously obtained for an Hamiltonian system (Lega et al., 2003). Moreover, we have shown that the phenomenon of Arnold's diffusion may also play an important role in the long-term evolution of quasi-integrable systems. More precisely the orbits can diffuse in a macroscopic portion of the phase space following in a spectacular way the peculiar structure of resonant lines.

References

Arnold, V. I.: 1964, 'Instability of dynamical systems with several degrees of freedom', *Sov. Math. Dokl.* **6**, 581–585.

Benettin, G. and Fassó, F.: 1999, 'From Hamiltonian perturbation theory to symplectic integrators and back', *App. Numer. Math.* **29**, 73–87.

Chirikov, B. V.: 1979, 'An universal instability of many dimensional oscillator system', *Phys. Rep.* **52**, 263–379.

Froeschlé, C., Lega, E. and Gonczi, R.: 1997, 'Fast Lyapunov indicators. Application to asteroidal motion', C*elest. Mech. Dyn. Astron.* **67,** 41–62.

Froeschlé, C., Guzzo, M. and Lega, E.: 2000, 'Graphical evolution of the Arnold's web: from order to chaos', *Science* **289(**N.5487), 2108–2110.

Froeschlé, C. and Lega, E.: 2000, 'On the structure of symplectic mappings. The fast Lyapunov indicator: a very sensitive tool', C*elest. Mech. Dyn. Astron.,* **78**, 167–195.

Froeschlé, C. and Lega, E.: 2005, 'The fast Lyapunov indicator. Applications to the study of the fine structure of Hamiltonian systems and to the detection of Arnold's diffusion', In: *Hamiltonian Systems and Fourier analysis*. New Prospectus for gravitational Dynamics, Cambridge Scientific Publishers.

Giorgilli, A. and Morbidelli, A.: 1997, *ZAMP*. **48**, 102–134.

Guzzo, M., Lega, E. and Froeschlé, C.: 2002,'On the numerical detection of the effective stability of chaotic motions in quasi-integrable systems', *Physica D* **163**, 1–25.

Guzzo, M.: 2004, 'A direct proof of the Nekhoroshev theorem for nearly integrable symplectic maps', *Ann. Henry poincaré*, **5**, 1013–1039.

Guzzo, M., Lega E. and Froeschlé, C.: 2005, 'First numerical evidence of global Arnold diffusion in quasi-integrable systems', DCDSB, in press.

Kuksin, S. and Pöschel, J.: 'On the inclusion of analytic symplectic maps in analytic Hamiltonian flows and its applications', Seminar on Dynamical Systems (St. Petersburg, 1991), 96–116. Progr. *Nonlinear Differential Equations Appl.* **12,** Birkhäuser, Basel.

Lega E., Guzzo, M. and Froeschlé, C.: 2003, 'Detection of Arnold diffusion in Hamiltonian systems', *Physica D* **182,** 179–187.

Morbidelli, A. and Giorgilli, A.: 1995, *Physica D* **86**, 514–516.

Nekhoroshev, N. N.: 1977, 'Exponential estimates of the stability time of near-integrable Hamiltonian systems', *Russ. Math. Surv.* **32,** 1–65.

Zaslavski, G. M. and Edelman, M.: 2000, 'Hierarchical structures in the phase space and fractional kinetics : I classical systems', *Chaos* **10**, 135–145.

Zaslavski, G. M. and Edelman, M.: 2001, 'Weak mixing and anomalous kinetics along filamented surfaces', Chaos **11**, 295–305.